RSC Advances

This is an *Accepted Manuscript*, which has been through the Royal Society of Chemistry peer review process and has been accepted for publication.

Accepted Manuscripts are published online shortly after acceptance, before technical editing, formatting and proof reading. Using this free service, authors can make their results available to the community, in citable form, before we publish the edited article. This *Accepted Manuscript* will be replaced by the edited, formatted and paginated article as soon as this is available.

You can find more information about *Accepted Manuscripts* in the Information for Authors.

Please note that technical editing may introduce minor changes to the text and/or graphics, which may alter content. The journal's standard Terms & Conditions and the Ethical guidelines still apply. In no event shall the Royal Society of Chemistry be held responsible for any errors or omissions in this *Accepted Manuscript* or any consequences arising from the use of any information it contains.

ROYAL SOCIETY OF CHEMISTRY

www.rsc.org/advances

Please do not adjust margins

Journal Name

COMMUNICATION

Gram-scale synthesis of high-purity graphene quantum dots with multicolor photoluminescence

Received 00th January 20xx,
Accepted 00th January 20xx

DOI: 10.1039/x0xx00000x

www.rsc.org/

Fuchi Liu,[a,b] Yuanyuan Sun,[a] Yongping Zheng,[a] Nujiang Tang,[*a] Ming Li,[a] Wei Zhong[a] and Youwei Du[a]

A gram-scale approach has been developed to prepare highly pure graphene quantum dots (GQDs) from Vulcan XC-72 carbon black by refluxed with concentrated nitric acid through a home-built experiment system. The weight of GQDs is high up to 1.2 g in each run with the yield of 75 wt. %, and the purity is 99.96 wt. %. The results show that GQDs exhibit multicolor photoluminescence from green to light red under different excitation wavelength.

Graphene quantum dots (GQDs) have aroused tremendous interest in nanoscience and nanotechnology due to their unique properties, such as the large surface area, low cytotoxicity, excellent solubility, a tunable bandgap,[1,2] quantum confinement and edge effects,[3,4] *etc.* GQDs are emerging as the promising nanomaterials for prospective applications in biological imaging and labeling,[5-9] ultrasensitive sensor and detection,[10-16] photoluminescent probes,[17] supercapacitors,[18-20] and solar cells,[21-23] *etc.* It's worth noting that for the biological applications of carbon nanomaterials in such as imaging receptors on living cells,[24] molecular diagnostics systems and nanotechnological research,[25] *etc.* the high purity is essential.

Recently, a variety of methods have been reported to synthesize GQDs, including microwave,[2] hydrothermal,[4] electrochemical,[26] and high-resolution electron-beam[27] approaches, and so on. Generally, these means suffered from the use of expensive materials such as graphene oxide (GO), reduced GO, or carbon fibre as precursor, and the yields of GQDs obtained are very low (<5 wt%), which limits the spread and applications of GQDs.[28] Moreover, some efforts had been taken to develop new methods to the high-yield synthesis of GQDs in recent years. For example, Sun *et al.* synthesized GQDs by the oxidation of natural graphite powder.[28] Shin *et al.* reported the one-pot synthesis of GQDs by high-powered microwave irradiation of graphite.[1] liu *et al.* synthesized gram-scale GQDs from active carbon atoms by Hummer's method.[29] Wang *et al.* reported a gram-scale synthesis of single-crystalline GQDs by a molecular fusion route under hydrothermal conditions, and the synthesis involves the nitration of pyrene followed by hydrothermal treatment in alkaline aqueous solutions.[30] However, the purity of the GQDs is low. Thus, the purification of GQDs obtained is needed, and which typically requires a very long time to ensure acid or alkali removal. More importantly, purification always involves a process that requires a strong base or acid, resulting in the introduction of a large amount of salt in GQDs. To obtain the high-purity GQDs, Dong *et al.* reported the synthesis of GQDs from carbon black by refluxed with concentrated nitric acid without using any other reagent.[31] Therein, the yield of the GQDs is still low. Thus, it is of great significance to develop a method for the synthesis of GQDs with both high yield and high purity.

Additionally, multicolor fluorescent nanomaterials have aroused continual interest. Typically, considerable studies have been focused on enhancing the multicolor photoluminescence (PL) or photodetection of fluorescent materials by means of graphene-base materials. For example, Zhu *et al.* developed a new strategy for multiple oligonucleotide target detection with three dye-labeled nucleic acid probes and GO.[32] Zhou *et al.* successfully designed an effective theranostic platform with multicolor imaging and satisfactory photo-induced anticancer activity based on porous silica nanoparticles encapsulated with the complex of a photodynamic anticancer drug and GQDs.[33] Notably, little work has been done on the multicolor optical properties of GQDs.

Herein, we report a gram-scale synthesis of highly pure GQDs from Vulcan XC-72 carbon black (Cabot Corporation). The results show that 1.2 g GQDs with the high yield of 75 wt. % and the high purity of 99.96 wt. % can be obtained in each run. More interesting, the GQDs show multicolor PL from green to light red.

As illustrated in Fig. 1a, GQDs were prepared by a modified Dong's methods [31] by a home-built experiment system. The main

[a] *Nanjing National Laboratory of Microstructures & Collaborative Innovation Center of Advanced Microstructures, Nanjing University, Nanjing 210093, People's Republic of China. tangnujiang@nju.edu.cn.*
[b] *College of Physics and Technology, Guangxi Normal University, Guilin 541004, People's Republic of China.*
†Electronic Supplementary Information (ESI) available:See
DOI: 10.1039/x0xx00000x

RSC Advances Accepted Manuscript

Please do not adjust margins

changes are shown below: (i) 15 mol L^{-1} HNO_3 was used to increase the oxidation capacity; (ii) The ethylene glycol was use to replace the water as coolant and was cooled at -5 ^{o}C by the low-temperature constant temperature bath to increase the reflux efficiency; (iii) 220 and 25 nm microporous membrane was used successively to remove the unoxidized carbon black or the big particle; (iv) The integrative home-built experiment system ensures the oxidation of carbon black and the evaporation of the nitric acid process can be finished under a situ and eco-friendly condition. Fig. 1b shows the schematics of the mechanism for the GQD formation from spherical carbon black. In a typical procedure, 1.6 g dried XC-72 carbon black and 300 ml 15 mol L^{-1} HNO_3 was put into a 1000 ml round bottom flask. The switch 1, 2, and 3 were opened and the switch 4 and 5 were shut. Then, the mixture was heated in an oil bath at 135 ^{o}C followed by refluxing and magnetic stirring for 24 h. At the same time, the condenser tube was cooling at -5 ^{o}C by the cryogenic ethylene glycol. To prevent the splattering of the hot oil, a specially designed water withdrawal device was used to remove the condensate water attached at the condenser tube. After refluxing for 24 h, the switch 1, 2, and 3 were turned off, and the switch 4 and 5 were turned on. The mixture was heated at 180 ^{o}C for approximately 10 h in a flowing Ar atmosphere (60 ml/min) to evaporate the concentrated nitric acid, and a small pile of light black solid was obtained. Thereafter, the solid was redissolved in 2 L deionized water (Fig. S1a†), and then the solution was centrifuged (13000 rpm) for 30 min to remove the unoxidized carbon black or the big particle. The obtained supernatant was vacuum filtered by 220 and 25 nm microporous membrane successively, and the unoxidized carbon black or the big particle was collected on the membrane (Fig. S1b-c†). Subsequently, the obtained reddish-brown GQDs solution (Fig. S1d†) was evaporated by rotary evaporators at 80 ^{o}C. After the obtained approximately 200 ml concentrated GQDs solution was dried by vacuum freeze drier, 1.2 g claybank powdered GQDs (Fig. 1c) were obtained. Note that, the weight is 13.5 times higher than that of reported GQDs (*ca.* 0.089 g).[31]

Fig. 2a and 2b show the typical Transmission electron microscopy (TEM) image and diameter distribution of GQDs. It is found that GQDs are relatively uniform with diameters of about 2-6 nm. According to the calculations, one can find that the average diameter of GQDs is *ca.* 4.2 nm (Fig. 2 b), obviously smaller than that of previous reported (*ca.* 15 nm).[31] Inset of Fig. 2a shows a HR-TEM image of GQD, which shows that it has discernible lattice structure. Fig. 2c, 2d, and 2e present an atomic force microscope (AFM) image of the GQDs, their height distribution, and the height line profile, respectively. One can see that the average height of the GQDs is *ca.* 1.05 nm, and more than 89% of the GQDs are less than 2 nm in height. It demonstrates that the obtained GQDs primarily consist of 1-3 layers.[26,34]

Fig. 3a show the Raman spectrum of the GQDs. One can see that there are two prominent peaks of the D and G band at 1366 and 1590 cm^{-1}, respectively. It is known that the D band is disordered band arising from the disorder in sp^2 hybridized carbon, while G band corresponds to the first-order scattering of the stretching vibration mode E_{2g} observed for sp^2 carbon domains.[35] The broad bands centered at 2680 and 2935 cm^{-1} correspond to the 2D and D+G bands, respectively.[36] They arise from the relaxation in selection rules caused by phonon scattering at boundaries and defects in GQDs.[35,37] Based on the Raman spectrum, one can find that the intensity ratio of D band to G band (I_D/I_G) is about 0.81. As reported by Tuinstra and Koenig,[38] I_D/I_G varies inversely with the cluster size L_a in nanocrystalline graphite according to this relationship: $I_D/I_G = C(\lambda)/ L_a$, where $C(\lambda)$ is an empirical constant that depends on the excitation laser energy and C (λ= 515.5 nm) = 4.4 nm.[38,39] According to this relation, the average size of the GQDs is L_a = 5.4 nm, which falls within the 2-6 nm range obtained by TEM data described above.

To detect the composition of the GQDs, X-ray photoemission spectroscopy (XPS) measurement was employed. Based on the XPS results (Fig. 3b), it is found that GQDs are oxygen-rich with a high oxygen content defined as 100 O/C at.% of *ca.* 53.7 at.%. The high-resolution C 1s peaks of GQDs can be deconvoluted into several peaks corresponding to the C-C bond in aromatic rings (284.6 eV), C–O bond (286.3 eV), and C=O bond (288.4 eV).[26] In addition, a little peak corresponding to the C–N bond (285.2 eV) also can be detected.

To evaluate the purity of the obtained GQDs, a contrastive GQDs was prepared by the universal hydrothermal method[4] from GO sheets, which was named as GQDs-1. Table 1 shows the impurity elements contens of GQDs and GQDs-1. One can see that the impurity elements contents (such as Fe, Ni, Mn, and Cu) of GQDs are much lower than those of GQDs-1. In particular, the contents of Na and Ca elements which may inevitably be introduced from the deionized water used during the preparation process are only 130.7 and 270.5 ppm for GQDs, respectively. By contrast, in the case of GQDs-1, they are high up to 10330 and 44030 ppm, which are ca. 80 and 163 times higher than those of GQDs. The reasons may be that (i) the synthesis of GQDs-1 involves a neutralization process which requires a strong base; and (ii) the concentration process for concentrating much water solution after dialysis, resulting in the introduction of a large amount of salt. Clearly, all the results indicate that the purity of our GQDs is much higher than that of GQDs prepared by the universal hydrothermal method. Namely, we have synthesized GQDs with high yield and purity through one-step chemical oxidation by our home-built experiment system.

For spectra investigation, 0.05 mg per 1 ml of sample solution was made by ultrasonically dispersed the solid GQDs in distilled water. As shown in Fig. 4a, the GQDs show a broad UV-vis absorption below 600 nm with one peak at ca.200 nm, and with three shoulder at ca. 225, 300, and 440 nm, respectively. Clearly, it is great different from that of GQDs previous reported.[31] Considering the fact that the size of our GQDs is obviously smaller than that of previous reported, the size effect may be responsible for the observed difference of the UV-vis absorption spectrum.

Fig. 4b shows the detailed PL of the GQDs. One can find that the GQDs exhibit an excitation-independent PL behavior with a emission peak position at 523 nm when the excitation wavelengths changed from 260 to 470 nm. By contrast, when the excitation wavelength changed from 470 to 580 nm, the maximum emission peak position shifted from 523 to 620 nm with red-shift about100 nm, showing clear excitation wavelength dependence. In brief, the GQDs have preeminent multicolor fluorescent emission depending on different excitations. Furthermore, the full width at a half maximum (FWHM) at excitation of 470 nm is only 110 nm, confirming the narrow size distribution of as-prepared GQDs

RSC Advances Accepted Manuscript

This journal is © The Royal Society of Chemistry 20xx

further. The multicolor photoluminescent feature of GQDs was also observed under different excitation wavelength through fluorophotometer. As shown in the inset of Fig. 4a, the solution of GQDs exhibits green, yellow green, yellow, orange and light red PL, respectively, under ultraviolet to blue (260–500 nm), green (510–530 nm), dark green (540–550 nm), yellow green (555–570 nm) and yellow (580–595 nm) light excitation, respectively. It should be noted that as the excitation wavelength red-shifted, the emission wavelength could reach light red regions. It suggests that our GQDs can be used in cell imaging.[40] The origins of PL in GQDs are not clear so far. One can propose that this observed multicolor PL may attribute to the different distribution of emissive traps on the surface of GQDs, as suggested in the literatures.[41,42]

The quantum yield (QY) of GQDs was assumed by using quinine sulfate as a reference (Table 2). It was calculated according to

$$\phi = \phi_r (I / I_r)(n^2 / n_r^2)(A_r / A)$$

where ϕ is the QY, *I* is the measured integrated emission intensity, *n* is the refractive index (1.33 for water), and *A* is the optical density. The subscript "*r*" refers to the reference of known QY. The QY of GQDs can be calculated to be *ca.* 5.1% by using quinine sulfate as a reference.

Conclusions

We reported a one-step pathway for the gram-scale synthesis of high-purity GQDs by refluxing Vulcan XC-72 carbon black with concentrated nitric acid through a home-built experiment system. The results showed that the yield of GQDs is high up to 1.2 g in each run by using 1.6 g XC-72 carbon black as starting material, and the purity is 99.96 wt. %. It is found that GQDs show evident multicolor PL feature. All the results suggest that the high-purity GQDs with multicolor PL hold great potential for optoelectronic and biomedical applications.

Acknowledgements

This work was financially supported by the State Key Program for Basic Research (Grant Nos. 2014CB921102 and 2012CB932304), NSFC (Grant Nos. U1232210 and 11164003), Guangxi Natural Science Foundation(Grant No.2015GXNSFAA139015), Foundation of Guangxi Educational Committee (Grant No. KY2015YB036), and Key Programs of Guangxi Normal University (Grant No. 2014ZD003), P. R. China.

Notes and references

1 Y. Shin, J. Lee, J. Yang, J. Park, K. Lee, S. Kim, Y. Park and H. Lee, *Small,* 2014, **10**, 866-870.
2 L. L. Li, J. Ji, R. Fei, C. Z. Wang, Q. Lu, J. R. Zhang, L. P. Jiang and J. J. Zhu, *Adv. Funct. Mater.,* 2012, **22**, 2971-2979.
3 X. Yan, X. Cui, B. Li and L. s. Li, *Nano Lett.,* 2010, **10**, 1869-1873.
4 D. Pan, J. Zhang, Z. Li and M. Wu, *Adv. Mater.,* 2010, **22**, 734-738.
5 H. Z. Pan, M. Xu, L. Chen, Y. Y. Sun and Y. L. Wang, *Acta Phys. Sinica,* 2010, **59**, 6443-6449.
6 Y. Wang, L. Zhang, R. P. Liang, J. M. Bai and J. D. Qiu, *Anal. Chem.,* 2013, **85**, 9148-9155.
7 S. Zhu, J. Zhang, C. Qiao, S. Tang, Y. Li, W. Yuan, B. Li, L. Tian, F. Liu, R. Hu, H. Gao, H. Wei, H. Zhang, H. Sun and B. Yang, *Chem. Commun.,* 2011, **47**, 6858-6860.
8 S. Chen, X. Hai, C. Xia, X. W. Chen and J. H. Wang, *Chem. Eur. J.,* 2013, **19**, 15918-15923.
9 X. T. Zheng, H. L. He and C. M. Li, *RSC Adv.,* 2013, **3**, 24853-24857.
10 J. J. Lu, M. Yan, L. Ge, S. G. Ge, S. W. Wang, J. X. Yan and J. H. Yu, *Biosensors & Bioelectronics,* 2013, **47**, 271-277.
11 Z. S. Qian, X. Y. Shan, L. J. Chai, J. J. Ma, J. R. Chen and H. Feng, *Biosensors & bioelectronics,* 2014, **60**, 64-70.
12 H. J. Sun, N. Gao, L. Wu, J. S. Ren, W. L. Wei and X. G. Qu, *Chem. Eur. J.,* 2013, **19**, 13362-13368.
13 C. Zhou, W. Jiang and B. K. Via, *Colloids and Surfaces B:Biointerfaces,* 2014, **118**, 72-76.
14 H. Sun, L. Wu, W. Wei and X. Qu, *Mater. Today,* 2013, **16**, 433-442.
15 J. P. Tian, H. M. Zhao, X. Quan, Y. B. Zhang, H. T. Yu and S. Chen, *Sensors and Actuators B,* 2014, **196**, 532-538.
16 F. X. Wang, Z. Y. Gu, W. Lei, W. J. Wang, X. F. Xia and Q. L. Hao, *Sensors and Actuators B,* 2014, **190**, 516-522.
17 J. M. Bai, L. Zhang, R. P. Liang and J. D. Qiu, *Chem. Eur. J.,* 2013, **19**, 3822-3826.
18 Y. Hu, Y. Zhao, G. Lu, N. Chen, Z. Zhang, H. Li, H. Shao and L. Qu, *Nanotechnology,* 2013, **24**, 1-7.
19 W. Liu, X. Yan, J. Chen, Y. Feng and Q. Xue, *Nanoscale,* 2013, **5**, 6053-6062.
20 W. W. Liu, Y. Q. Feng, X. B. Yan, J. T. Chen and Q. J. Xue, *Adv. Funct. Mater.,* 2013, **23**, 4111-4122.
21 J. K. Kim, M. J. Park, S. J. Kim, D. H. Wang, S. P. Cho, S. Bae, J. H. Park and B. H. Hong, *ACS Nano,* 2013, **7**, 7207-7212.
22 Z. L. Zhu, J. A. Ma, Z. L. Wang, C. Mu, Z. T. Fan, L. L. Du, Y. Bai, L. Z. Fan, H. Yan, D. L. Phillips and S. H. Yang, *J. Am. Chem. Soc.,* 2014, **136**, 3760-3763.
23 H. B. Yang, Y. Q. Dong, X. Z. Wang, S. Y. Khoo, B. Liu and C. M. Li, *Solar Energy Materials & Solar Cells,* 2013, **117**, 214-218.
24 M. Howarth, W. Liu, S. Puthenveetil, Y. Zheng, L. F. Marshall, M. M. Schmidt, K. D. Wittrup, M. G. Bawendi and A. Y. Ting, *Nat. Meth.,* 2008, **5**, 397-399.
25 P. M. E. Gramlich, C. T. Wirges, A. Manetto and T. Carell, *Angew. Chem. Int. Ed.,* 2008, **47**, 8350-8358.
26 Y. Li, Y. Hu, Y. Zhao, G. Shi, L. Deng, Y. Hou and L. Qu, *Adv. Mater.,* 2011, **23**, 776-780.
27 L. A. Ponomarenko, F. Schedin, M. I. Katsnelson, R. Yang, E. W. Hill, K. S. Novoselov and A. K. Geim, *Science,* 2008, **320**, 356-358.
28 Y. Sun, S. Wang, C. Li, P. Luo, L. Tao, Y. Wei and G. Shi, *Phys. Chem. Chem. Phys.,* 2013, **15**, 9907-9913.
29 Y. Liu, B. Gao, Z. Qiao, Y. Hu, W. Zheng, L. Zhang, Y. Zhou, G. Ji and G. Yang, *Chem. Mater.,* 2015, **27**, 4319-4327.
30 L. Wang, Y. Wang, T. Xu, H. Liao, C. Yao, Y. Liu, Z. Li, Z. Chen, D. Pan, L. Sun and M. Wu, *Nat Commun,* 2014, **5**.

RSC Advances Accepted Manuscript

31 Y. Dong, C. Chen, X. Zheng, L. Gao, Z. Cui, H. Yang, C. Guo, Y. Chi and C. M. Li, *J. Mater. Chem.,* 2012, **22**, 8764-8766.

32 Q. Zhu, D. Xiang, C. Zhang, X. Ji and Z. He, *Analyst,* 2013, **138**, 5194-5196.

33 L. Zhou, X. Ge, J. Zhou, S. Wei and J. Shen, *Chem. Commun.,* 2015, **51**, 421-424.

34 X. Li, X. Wang, L. Zhang, S. Lee and H. Dai, *Science,* 2008, **319**, 1229-1232.

35 A. C. Ferrari and J. Robertson, *Phys. Rev. B,* 2000, **61**, 14095-14107.

36 K. Habiba, V. I. Makarov, J. Avalos, M. J. F. Guinel, B. R. Weiner and G. Morell, *Carbon,* 2013, **64**, 341-350.

37 P. Lespade, R. Al-Jishi and M. Dresselhaus, *Carbon,* 1982, **20**, 427-431.

38 F. Tuinstra and J. L. Koenig, *J. Chem. Phys.,* 1970, **53**, 1126.

39 M. S. Dresselhaus, A. Jorio, A. G. Souza Filho and R. Saito, *Philos Trans R Soc A,* 2010, **368**, 5355-5377.

40 C. Liu, P. Zhang, F. Tian, W. Li, F. Li and W. Liu, *J. Mater. Chem.,* 2011, **21**, 13163-13167.

41 R. Liu, D. Wu, S. Liu, K. Koynov, W. Knoll and Q. Li, *Angew. Chem. Int. Ed.,* 2009, **48**, 4598-4601.

42 L. Zheng, Y. Chi, Y. Dong, J. Lin and B. Wang, *J. Am. Chem. Soc.,* 2009, **131**, 4564-4565.

RSC Advances Accepted Manuscript

This journal is © The Royal Society of Chemistry 20xx

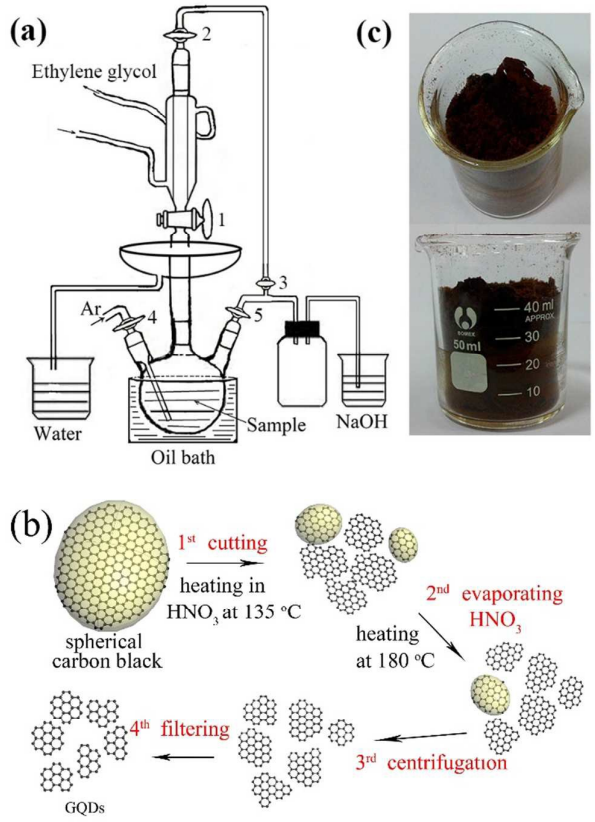

Fig. 1 (a) Schematic illustration of the home-built experiment system. (b) Schematics of the mechanism for the GQD formation.(c) Top and front views of 1.2 g powdered GQDs obtained by one run.

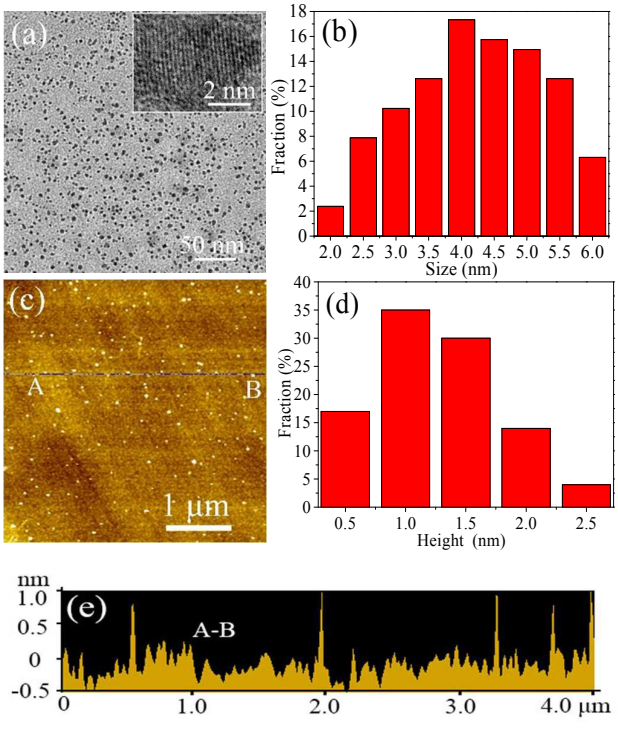

Fig. 2 Microstructure of the as-prepared GQDs: (a) TEM image. Inset of (a): HR-TEM image. (b) Diameter distribution. (c) AFM image. (d) Height distribution. (e) Height profile along the line A–B.

Table 1 Inductively coupled plasma (ICP) analysis data of GQDs.

Samples(ppm)	Fe	Ni	Mn	Cu	Na	Ca
GQDs	2.6	0.8	0.8	3.6	130.7	270.5
GQDs-1	96.3	11.1	38.3	18.5	10330	44030

Table 2 QY of GQDs using quinine sulfate as a reference.

Sample	Integrated emission intensity (I)	Abs. (A)	Refractive index of solvent (n)	Quantum yield (ϕ)
Quinine sulfate	65134.5	0.0523	1.33	0.54 (known)
GQDs	4321.6	0.0371	1.33	0.051

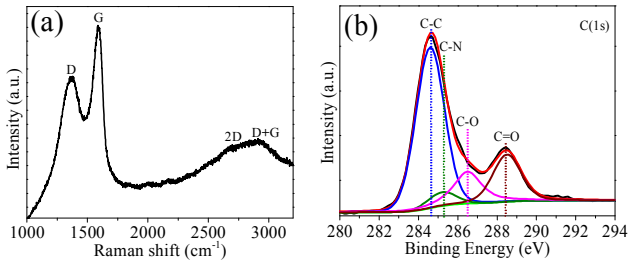

Fig. 3 (a) Raman spectrum of the GQDs. (b) XPS spectrum of the GQDs.

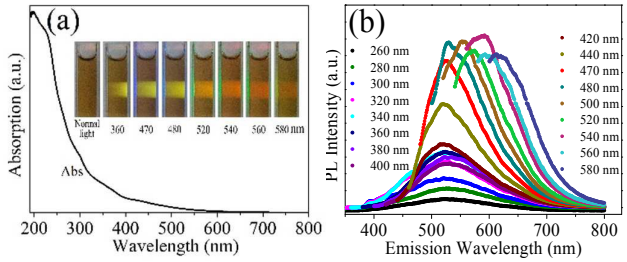

Fig. 4 (a) UV-vis absorption spectrum of the GQDs at different excitation wavelengths. Inset: Optical photograph of the GQDs dispersed in water under different wavelengths irradiation. (b) PL spectra of the GQDs at excitation wavelengths from 260 to 580 nm.

RSC Advances Accepted Manuscript